PHYSICAL REVIEW B **89**, 220510(R) (2014)

Pairing symmetry and dominant band in Sr_2RuO_4

Thomas Scaffidi, Jesper C. Romers, and Steven H. Simon
Rudolf Peierls Centre for Theoretical Physics, Oxford OX1 3NP, United Kingdom

(Received 31 December 2013; revised manuscript received 16 June 2014; published 27 June 2014)

We study the superconductivity pairing symmetry in Sr_2RuO_4 in the limit of small interaction by extending a renormalization group calculation developed by Raghu *et al.* [Phys. Rev. B **81**, 224505 (2010)] to include spin-orbit coupling and multiband effects. We show these effects to be crucial to discriminate between the possible order parameters. In contrast to previous results and without the necessity of fine-tuning, we obtain pseudospin-triplet gaps of the same order of magnitude on the two-dimensional $\boldsymbol{\gamma}$ band and the quasi-one-dimensional $\boldsymbol{\alpha}$ and $\boldsymbol{\beta}$ bands. The ratio of the gap amplitude on the different bands varies continuously with the interaction parameter. The favored pairing symmetry is shown to be chiral when $\boldsymbol{\gamma}$ is slightly dominant and helical when $\boldsymbol{\alpha}$ and $\boldsymbol{\beta}$ are slightly dominant.

DOI: 10.1103/PhysRevB.89.220510 PACS number(s): 74.70.Pq, 74.20.Mn, 74.20.Rp

Strontium ruthenate [1–3] is a layered perovskite material exhibiting a transition at 1.5 K from a well-behaved Fermi liquid to a superconducting phase. Strong experimental evidence points towards an odd-parity order parameter (OP) [4–7]. Based on multiple experiments [7–12], the prevailing candidate for the symmetry of the OP has been the chiral p-wave state, $\mathbf{d} = (p_x \pm ip_y)\hat{\mathbf{z}}$, which breaks time-reversal symmetry (TRS), hosts topologically protected chiral edge states, and is analogous to superfluid ^{3}He-A [13,14] ($\mathbf{d}$ is defined below).

On the other hand, this state is supposed to carry edge currents at sample edges and domain walls, which have been elusive so far despite intense scrutiny [15,16]. As a result, other OP symmetries have been considered theoretically [17–20], including the helical states, $\mathbf{d} = p_x\hat{\mathbf{x}} \pm p_y\hat{\mathbf{y}}$ and $\mathbf{d} = p_y\hat{\mathbf{x}} \pm p_x\hat{\mathbf{y}}$. These phases can be viewed as time-reversal invariant versions of chiral superconductors. Their edges host two counterpropagating Majorana modes of opposite spin whose net charge current is zero.

Another controversy has arisen recently regarding the band(s) on which the superconducting instability is dominant. The Fermi surface (FS) of Sr_2RuO_4 is made of three cylindrical sheets: The $\boldsymbol{\gamma}$ band is mainly derived from the Ru $4d_{xy}$ orbital and is fairly isotropic in the basal plane, while the $\boldsymbol{\alpha}$ and $\boldsymbol{\beta}$ bands are mainly derived from the Ru $4d_{xz}$ and $4d_{yz}$ orbitals and are quasi-one-dimensional (see Fig. 1).

The prevailing assumption in the field has been that $\boldsymbol{\gamma}$ is the active band, due to its proximity to a Van Hove singularity. This assumption was based on specific heat data [21] and backed by several calculations [22–26] that predicted a dominant gap on $\boldsymbol{\gamma}$ and a subdominant, near-nodal gap on $\boldsymbol{\alpha}$ and $\boldsymbol{\beta}$.

This scenario was challenged recently. First, Raghu *et al.* [27] (see also [28]) showed that, in absence of band coupling and in the weak-coupling limit, $\boldsymbol{\alpha}$ and $\boldsymbol{\beta}$ are the active bands. Second, Firmo *et al.* [29] reported a phenomenological model with a gap amplitude of similar size on the three bands but slightly larger on $\boldsymbol{\alpha}$ and $\boldsymbol{\beta}$ than on $\boldsymbol{\gamma}$ that is consistent with specific heat and scanning tunneling microscopy (STM) measurements.

In this Rapid Communication, we extend the renormalization group (RG) scheme of Raghu *et al.* [30–34] by including spin-orbit coupling [35,36] and multiband effects. This enables us to study the orientation of $\mathbf{d}$ at a microscopic level and determine the gap on the three bands. We find similarly sized gaps on the three bands without the necessity of fine-tuning. Depending on the interaction parameter, we find two OPs that are compatible with the thermodynamic data: either a chiral gap whose amplitude is slightly larger on $\boldsymbol{\gamma}$, or a helical gap whose amplitude is slightly larger on $\boldsymbol{\alpha}$ and $\boldsymbol{\beta}$.

The three bands of strontium ruthenate are reproduced using the following tight-binding Hamiltonian for electrons hopping on a square lattice [37,38]:

$$H = \sum_{\mathbf{k},s} \psi_s^\dagger(\mathbf{k})\hat{H}_s(\mathbf{k})\psi_s(\mathbf{k}), \tag{1}$$

where $\psi_s(\mathbf{k}) = [c_{\mathbf{k},A,s}; c_{\mathbf{k},B,s}; c_{\mathbf{k},C,-s}]^T$ with $s = 1\,(-1)$ for up (down) spins. The matrix $\hat{H}_s(\mathbf{k})$ is given by [39]

$$\hat{H}_s(\mathbf{k}) = \begin{pmatrix} E_A(\mathbf{k}) & g(\mathbf{k}) - si\eta & i\eta \\ g(\mathbf{k}) + si\eta & E_B(\mathbf{k}) & -s\eta \\ -i\eta & -s\eta & E_C(\mathbf{k}) \end{pmatrix}, \tag{2}$$

where $E_A(\mathbf{k}) = -2t\,\cos(k_x) - 2t^\perp\cos(k_y) - \mu$, $E_B(\mathbf{k}) = -2t^\perp\cos(k_x) - 2t\,\cos(k_y) - \mu$, $E_C(\mathbf{k}) = -2t'[\cos(k_x) + \cos(k_y)] - 4t''\cos(k_x)\cos(k_y) - \mu_c$, and $g(\mathbf{k}) = -4t'''\sin(k_x)\sin(k_y)$. A, B, and C stand for the Ru orbitals $4d_{xz}$, $4d_{yz}$, and $4d_{xy}$ on each lattice site. The spin-orbit coupling (SOC) parameter is η and the interorbital hopping term is $g(\mathbf{k})$ [40]. The parameters were chosen to reproduce the shape of the Fermi surfaces and the ratio of the effective masses of the different bands obtained from experiments [2,41]: In dimensionless units, $(t,t^\perp,t',t'',\mu,\mu_c,t''',\eta) = (1.0,0.1,0.8,0.3,1.0,1.1,0.01,0.1)$.

After diagonalization, we obtain three pairs of degenerate pseudospin bands:

$$H = \sum_{\mathbf{k},\alpha,\sigma} \epsilon_{\mathbf{k},\alpha} c^\dagger_{\mathbf{k},\alpha,\sigma} c_{\mathbf{k},\alpha,\sigma} \tag{3}$$

with $\sigma = 1\,(-1)$ for $+\,(-)$ pseudospin and $\alpha = \boldsymbol{\alpha},\boldsymbol{\beta},\boldsymbol{\gamma}$. Roman indices refer to spin and orbital space, while greek indices refer to pseudospin and band space.

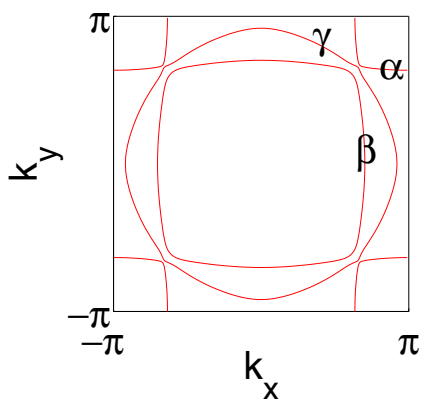

FIG. 1. (Color online) Fermi surfaces for the tight-binding model H given in Eq. (1).

We study the Coulomb interaction in the on-site d atomic orbitals basis:

$$H_{\text{int}} = \sum_{i,a,s\neq s'} \frac{U}{2} n_{ias} n_{ias'} + \sum_{i,a\neq b,s,s'} \frac{U'}{2} n_{ias} n_{ibs'} + \sum_{i,a\neq b,s,s'} \frac{J}{2} c^{\dagger}_{ias} c^{\dagger}_{ibs'} c_{ias'} c_{ibs} + \sum_{i,a\neq b,s\neq s'} \frac{J'}{2} c^{\dagger}_{ias} c^{\dagger}_{ias'} c_{ibs'} c_{ibs}, \quad (4)$$

where i is the site index, $a = A,B,C$ is the orbital index, $\overline{s} \equiv -s$, $n_{ias} \equiv c^{\dagger}_{ias} c_{ias}$, $U' = U - 2J$, and $J' = J$ [42].

Following Raghu *et al.* [30], we treat the weak-coupling limit, which corresponds to $U,J \ll W$ where W is the bandwidth and J/U a finite constant that fully parametrizes the interaction. This is a well-controlled approximation in the sense that the solutions obtained are asymptotically exact in the weak-coupling limit. However, all real systems have finite interaction strengths and one is therefore forced to extrapolate this technique's results out of its strict regime of validity in order to make a link with experiments. Although this extrapolation probably leads to quantitative changes in our results, it should leave the qualitative trends untouched.

We integrate out all the modes with energies greater than an artificial cutoff to derive the effective particle-particle interaction in the Cooper channel $V(\mathbf{k}_\alpha,\mathbf{q}_\beta)$, where $\epsilon_\alpha(\mathbf{k}_\alpha)$ lies below the cutoff. The effective interaction $V(\mathbf{k}_\alpha,\mathbf{q}_\beta)$ corresponds to the diagram depicted in Fig. 2(a). Its pseudospin dependence is left implicit for now. Besides the bare vertex and its ladder, which give a trivial repulsive contribution, the effective interaction at one-loop order is made of the three diagrams shown in Fig. 2(b). These diagrams are expressed in terms of the static susceptibility of the noninteracting system and correspond to the celebrated "Kohn-Luttinger" physics [43,44]. The different bare vertices given in Eq. (4) are represented diagrammatically by a unique dashed line that corresponds to a matrix in spin and orbital space. As the external propagators are in pseudospin and band space, the diagram expressions are supplemented by form factors

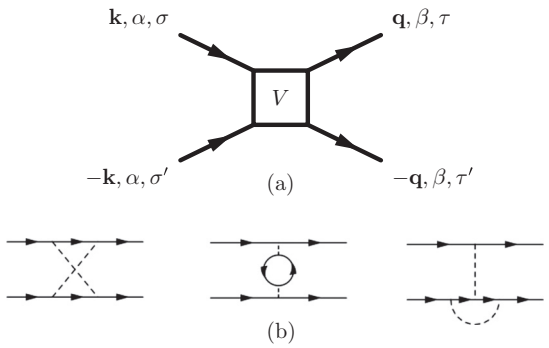

FIG. 2. (a) Diagram corresponding to the effective interaction $V(\mathbf{k}_\alpha,\mathbf{q}_\beta)$. (b) Nontrivial contribution to $V(\mathbf{k}_\alpha,\mathbf{q}_\beta)$ at one-loop order.

from the unitary transformation going from spin and orbital to pseudospin and band space.

The second stage of the weak-coupling analysis is the calculation of the RG flow [30]. Each eigenmode of the effective interaction flows independently under the evolution of the running cutoff. These eigenmodes are solutions of

$$\sum_\beta \int_{\text{FS}} \frac{d\mathbf{q}_\beta}{S_F} g(\mathbf{k}_\alpha,\mathbf{q}_\beta)\psi(\mathbf{q}_\beta) = \lambda\psi(\mathbf{k}_\alpha), \quad (5)$$

where

$$g(\mathbf{k}_\alpha,\mathbf{q}_\beta) = \sqrt{\rho_\alpha \frac{\overline{v_{F,\alpha}}}{v_F(\mathbf{k}_\alpha)}}\, V(\mathbf{k}_\alpha,\mathbf{q}_\beta) \sqrt{\rho_\beta \frac{\overline{v_{F,\beta}}}{v_F(\mathbf{q}_\beta)}}, \quad (6)$$

S_F is the "area" of the FS, ρ_α is the density of states (DOS) of the band α at the Fermi level, and the average of the norm of the Fermi velocity is given by

$$\overline{v_{F,\alpha}}^{-1} = \int \frac{d\mathbf{k}_\alpha}{S_F} v_F(\mathbf{k}_\alpha)^{-1}. \quad (7)$$

Since $\mathbf{k}_\alpha$ and $\mathbf{q}_\beta$ are constrained to lie on their respective FS, Eq. (5) is solved in matrix form once the FSs are discretized.

The energy scale at which the perturbative treatment of the interaction breaks down corresponds to the critical temperature and is given by [30]

$$T_c \sim W \exp\left(-\frac{1}{|\lambda|}\right). \quad (8)$$

The gap is proportional to the eigenvector [30]:

$$\Delta(\mathbf{k}_\alpha) \sim \sqrt{\frac{v_F(\mathbf{k}_\alpha)}{\overline{v_{F,\alpha}}\rho_\alpha}}\psi(\mathbf{k}_\alpha). \quad (9)$$

The pseudospin dependence of the order parameter is written in matrix form:

$$\Delta(\mathbf{k}_\alpha) = \begin{pmatrix} \Delta_{++} & \Delta_{+-} \\ \Delta_{-+} & \Delta_{--} \end{pmatrix} = \begin{pmatrix} -d_x + i d_y & d_z + \Delta_s \\ d_z - \Delta_s & d_x + i d_y \end{pmatrix}, \quad (10)$$

which defines a scalar order parameter Δ_s for the singlet case and a vectorial order parameter $\mathbf{d}$ for the triplet case. Since they are respectively even and odd under inversion, these two cases are mutually exclusive. The direction of $\mathbf{d}$ defines the normal to the plane in which the electrons are equal pseudospin paired.

The order parameter has to be in a given irreducible representation of the crystal symmetry group D_{4h}. The odd-parity representations can be split into two groups: the chiral state $\mathbf{d} = (p_x \pm ip_y)\hat{\mathbf{z}}$ and the helical states $\mathbf{d} = p_x\hat{\mathbf{x}} \pm p_y\hat{\mathbf{y}}$ and $\mathbf{d} = p_y\hat{\mathbf{x}} \pm p_x\hat{\mathbf{y}}$. The symbols $p_{x,y}$ stand for any function of momentum that has the same properties as $\sin(k_{x,y})$ under the symmetry operations of D_{4h}. The unit vectors $\hat{\mathbf{x}}$, $\hat{\mathbf{y}}$, and $\hat{\mathbf{z}}$ are the directions a [100], b [010], and c [001]. The representation with the most negative pairing eigenvalue λ corresponds to the favored state.

Since there is no consensus regarding the value of the interaction parameters [45], we will study *a priori* the whole acceptable range of J/U and then compare predictions with experiments to infer its possible value. The singlet case appears only for $J/U > 0.29$ and can be discarded based on multiple measurements [4–7]. While, for $J/U < 0.065$, the chiral state is favored in agreement with the most prevailing assumption in the field, the helical state $\mathbf{d} = p_x\hat{\mathbf{x}} + p_y\hat{\mathbf{y}}$ takes over for $0.065 < J/U < 0.29$. The helical state is the two-dimensional (2D) equivalent of superfluid ^{3}He-B [46].

The TRS obeyed by the helical state is in contradiction with muon spin relaxation [8] and optical Kerr effect [10] experiments but the interpretation of these experiments appears to conflict with the absence of edge currents [47,48]. The absence of spin susceptibility decrease below T_c for both in-plane and out-of-plane fields measured by NMR Knight shift experiments [4,49] has been interpreted as evidence in favor of a weakly pinned $\mathbf{d} \parallel c$ that can be rotated to the plane by a field $h \parallel c$ smaller than 20 mT. We emphasize that a helical state with a weakly pinned $\mathbf{d} \perp c$ that would be rotated by a field $h \parallel ab$ smaller than 150 mT would also be consistent with these experiments.

Furthermore, the helical state would provide a simple explanation for the presence of edge states [50] but the absence of edge currents [15,16]. It would also explain the emergence of out-of-plane spin fluctuations in the superconducting state [51,52], which require in-plane fluctuations of $\mathbf{d}$. The disappearance of these fluctuations under an in-plane magnetic field would also be consistent with the expulsion of $\mathbf{d}$ from the plane under such a field. Half-quantum vortices, measured recently in a mesoscopic sample of Sr_2RuO_4 [53], correspond to a spatially dependent rotation of $\mathbf{d}$ in order to accommodate a half-integer flux. They require a freeing of $\mathbf{d}$ from its intrinsic direction imposed by SOC and their existence is therefore equally plausible in the chiral and the helical state. Given these contradictory experimental results, we will study these two states on an equal footing.

Once the mode with the most negative eigenvalue is identified, its eigenvector provides valuable information regarding the gap. The gap scale is too small to be measured directly by angle-resolved photoemission spectroscopy (ARPES) but specific heat measurements have revealed properties of the order parameter [29,54]. In Fig. 3, we compare the measured [55] critical jump in specific heat $\frac{\Delta C}{C}$ with its value calculated using BCS theory on the gap functions obtained from the RG technique. The two highlighted regions correspond to a prediction for $\frac{\Delta C}{C}$ in agreement with experiments: the chiral OP at $J/U \simeq 0.06$ and the helical OP at $J/U \simeq 0.08$.

The departure of $\frac{\Delta C}{C}$ from its well-known BCS maximal value of 1.43 measures the anisotropy of the gap over the three FS. A large difference between the scale of the gap amplitudes on the different bands corresponds to a value of $\frac{\Delta C}{C}$ that is smaller than experiments, as can be seen in Fig. 3. Accordingly, the two predicted OPs in agreement with specific heat data have gaps of the same order on the three bands. The slightly dominant band is different in the two cases: The chiral state has a gap approximately two times larger on $\boldsymbol{\gamma}$ than on $\boldsymbol{\alpha}$ and $\boldsymbol{\beta}$, while the ratio of the helical gap amplitude on $\boldsymbol{\gamma}$ over the one on $\boldsymbol{\alpha}$ and $\boldsymbol{\beta}$ is approximately 0.7. We checked that both these states give rise to a T linear dependence of C/T below T_c, in agreement with experiments [55]. By tuning J/U towards smaller values, it is possible to obtain a largely dominant gap on $\boldsymbol{\gamma}$ like previously reported [22–26].

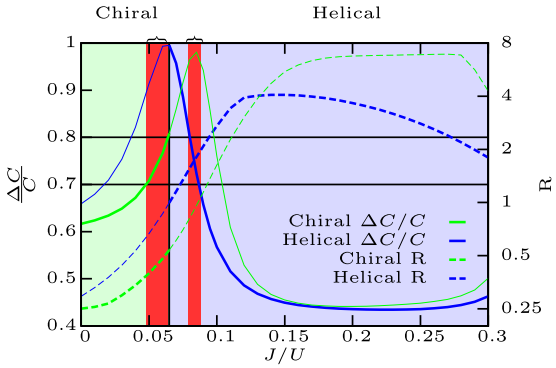

FIG. 3. (Color online) Critical specific heat jump $\frac{\Delta C}{C}$ and ratio of the maxima of the gap amplitudes over the different bands $R = \frac{\max|\Delta_{\alpha,\beta}|}{\max|\Delta_\gamma|}$. The vertical line separates the stability regions of the chiral and helical OPs. The curve for a given OP is drawn in full width only in the OP's stability region. The horizontal lines delimit the range of $\frac{\Delta C}{C}$ estimated from experiments: $\frac{\Delta C}{C} = 0.75 \pm 0.05$ [29,55]. The braces indicate the range of J/U for which the prediction is in agreement with experiments.

As shown in Fig. 4, the gaps on $\boldsymbol{\alpha}$ and $\boldsymbol{\beta}$ present near nodes near the direction [110] in both cases. The incommensurate peak $\mathbf{Q}$ in the antiferromagnetic fluctuation spectrum [56] of these bands is known to be responsible for the appearance of these near nodes [27,29]. As its fluctuations are mostly ferromagnetic, the $\boldsymbol{\gamma}$ band has been previously thought to host a fairly isotropic gap of the type $d_z = \sin(k_x) + i\ \sin(k_y)$, with only mild minima along [100] [22–26] and a complex phase increasing quasilinearly with θ (defined in Fig. 4). Interestingly, we find gap minima on $\boldsymbol{\gamma}$ along [110], which shows that the quasi-one-dimensional (quasi-1D) antiferromagnetic fluctuations peak $\mathbf{Q}$ is a source of anisotropy on this band as well. Besides, the complex phase of our solution for d_z in the chiral case [shown in Fig. 4(c)] is a highly nontrivial and nonmonotonic function of θ. Likewise, the in-plane orientation of $\mathbf{d}$ as a function of θ in the helical case [shown in Fig. 4(d)] is much more involved than for the archetypal function $\mathbf{d} = \sin(k_x)\hat{\mathbf{x}} + \sin(k_y)\hat{\mathbf{y}}$.

The rationale behind the association of the chiral state with a dominant $\boldsymbol{\gamma}$ and the helical state with dominant $\boldsymbol{\alpha}$ and $\boldsymbol{\beta}$ lies in the anisotropy of the normal-state spin dynamics. The chiral (helical) state has an out-of-plane (in-plane) $\mathbf{d}$ and is therefore driven by in-plane (out-of-plane) magnetic fluctuations. Due to SOC, the incommensurate peak $\mathbf{Q}$ is larger for the out-of-plane

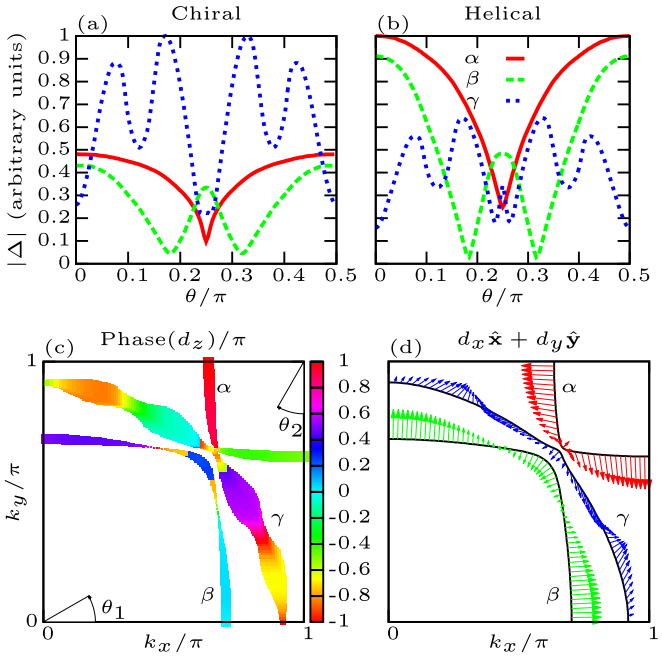

FIG. 4. (Color online) We represent the chiral OP $\mathbf{d} = d_z\hat{\mathbf{z}}$ for $J/U = 0.06$ (left) and the helical OP $\mathbf{d} = d_x\hat{\mathbf{x}} + d_y\hat{\mathbf{y}}$ for $J/U = 0.08$ (right). Panels (a) and (b) show the gap magnitude $|\Delta| \equiv \sqrt{\mathbf{d}\cdot\mathbf{d}^*}$. In panel (c), the color code gives the complex phase of d_z around the three FSs. The width of the curve is proportional to $|\Delta|$. In panel (d), the vectors are proportional to (d_x, d_y), where d_x and d_y are real. The angle θ refers to θ_1 (θ_2) in the case of β and γ (α).

component of the susceptibility [57], thereby favoring a helical state when the quasi-1D bands are dominant. On the other hand, the (ferromagnetic) long wavelength part of the spectrum is larger for the in-plane component, which favors a chiral state when $\boldsymbol{\gamma}$ is dominant.

By a microscopic accounting of multiband and SOC effects, our model reconciles the two distinct scenarios of 2D superconductivity on $\boldsymbol{\gamma}$ versus quasi-1D superconductivity on $\boldsymbol{\alpha}$ and $\boldsymbol{\beta}$ inside one framework. As required by specific heat data [29] and in contrast to previous RG calculations [26,27], similarly sized gaps on all three bands are obtained and, depending on the interaction parameter, the balance can be slightly tilted one way or another. As shown in Fig. 3, this result is true for both the chiral and the helical state and is therefore robust regardless of the favored pairing symmetry.

We now discuss experiments probing the relative size of the gaps on the different bands. Recently, out-of-plane STM [29] has exhibited the presence of a near-nodal gap of 0.350 meV on $\boldsymbol{\alpha}$ and $\boldsymbol{\beta}$. We find a position for the near nodes on $\boldsymbol{\alpha}$ and $\boldsymbol{\beta}$ that is consistent with their phenomenological model, and we could reproduce their experimental tunneling DOS curves based on our gap. Due to orbital anisotropy, the gap on $\boldsymbol{\gamma}$ cannot be measured with such an experiment. The fact that the measured gap size corresponds to $2\Delta/T_c \simeq 5$, which is close to the BCS value, was interpreted as evidence that $\boldsymbol{\alpha}$ and $\boldsymbol{\beta}$ are dominant. A gap 0.7 times smaller on $\boldsymbol{\gamma}$ was then inferred from the specific heat jump value, in agreement with our findings for the helical state.

On the other hand, the conductance of in-plane tunneling junctions [50] has been reported to present a two-step peak shape that is consistent with a dominant gap of 0.93 meV on $\boldsymbol{\gamma}$ and a subdominant gap of 0.28 meV on $\boldsymbol{\alpha}$ and $\boldsymbol{\beta}$. The relative sizes of the gap amplitude on the different bands would then point towards the chiral scenario.

The inclusion of η is crucial to study the orientation of $\mathbf{d}$ since, without SOC, the spin $SU(2)$ symmetry would be preserved and the chiral and helical states would be degenerate. The splitting between the pairing eigenvalue of these states grows with the magnitude of η but our conclusions are robust against a change in this parameter: The favored state is always chiral with a (slightly) dominant $\boldsymbol{\gamma}$ for small J/U and helical with (slightly) dominant $\boldsymbol{\alpha}$ and $\boldsymbol{\beta}$ for larger J/U (see Supplemental Material for more details [39]).

Finally, we emphasize the need for new experiments that would make it possible to discriminate between the two proposed states. In-plane STM could be one of them since it could also measure the gap on $\boldsymbol{\gamma}$ unlike in the out-of-plane case. Experiments probing the phase of the order parameter, including quasiparticle interference and Josephson tunneling spectroscopy [7,11,12], could be discriminating but their interpretation is nontrivial given the reported convoluted dependence of that phase on the in-plane orientation. Methods to detect helical edge modes have also been proposed recently [58].

Helpful conversations with Sri Raghu, Steve Kivelson, Suk Bum Chung, Andy Mackenzie, Andrew Green, Jonathan Keeling, Chris Hooley, Clifford Hicks, Ed Yelland, Jim Sauls, Catherine Kallin, Andrea Damascelli, and Peter Hirschfeld are acknowledged. This work is supported by EPSRC Grants No. EP/I032487/1 and No. EP/I031014/1, the Clarendon Fund Scholarship, and the University of Oxford.

[1] Y. Maeno, H. Hashimoto, K. Yoshida, S. Nishizaki, T. Fujita, J. Bednorz, and F. Lichtenberg, Nature (London) **372**, 532 (1994).

[2] A. P. Mackenzie and Y. Maeno, Rev. Mod. Phys. **75**, 657 (2003).

[3] Y. Maeno, S. Kittaka, T. Nomura, S. Yonezawa, and K. Ishida, J. Phys. Soc. Jpn. **81**, 011009 (2012).

[4] K. Ishida, H. Mukuda, Y. Kitaoka, K. Asayama, Z. Mao, Y. Mori, and Y. Maeno, Nature (London) **396**, 658 (1998).

[5] J. A. Duffy, S. M. Hayden, Y. Maeno, Z. Mao, J. Kulda, and G. J. McIntyre, Phys. Rev. Lett. **85**, 5412 (2000).

[6] K. D. Nelson, Z. Q. Mao, Y. Maeno, and Y. Liu, Science **306**, 1151 (2004).

[7] F. Kidwingira, J. D. Strand, D. J. Van Harlingen, and Y. Maeno, Science **314**, 1267 (2006).

[8] G. Luke, Y. Fudamoto, K. Kojima, M. Larkin, J. Merrin, B. Nachumi, Y. Uemura, Y. Maeno, Z. Mao, Y. Mori, H. Nakamura, and M. Sigrist, Nature (London) **394**, 558 (1998).

[9] P. G. Kealey, T. M. Riseman, E. M. Forgan, L. M. Galvin, A. P. Mackenzie, S. L. Lee, D. M. Paul, R. Cubitt, D. F. Agterberg, R. Heeb, Z. Q. Mao, and Y. Maeno, Phys. Rev. Lett. **84**, 6094 (2000).

[10] J. Xia, Y. Maeno, P. T. Beyersdorf, M. M. Fejer, and A. Kapitulnik, Phys. Rev. Lett. **97**, 167002 (2006).
[11] Y. Liu, New J. Phys. **12**, 075001 (2010).
[12] M. S. Anwar, T. Nakamura, S. Yonezawa, M. Yakabe, R. Ishiguro, H. Takayanagi, and Y. Maeno, Sci. Rep. **3**, 2480 (2013).
[13] P. W. Anderson and W. F. Brinkman, Phys. Rev. Lett. **30**, 1108 (1973).
[14] P. W. Anderson and P. Morel, Phys. Rev. **123**, 1911 (1961).
[15] J. R. Kirtley, C. Kallin, C. W. Hicks, E.-A. Kim, Y. Liu, K. A. Moler, Y. Maeno, and K. D. Nelson, Phys. Rev. B **76**, 014526 (2007).
[16] C. W. Hicks, J. R. Kirtley, T. M. Lippman, N. C. Koshnick, M. E. Huber, Y. Maeno, W. M. Yuhasz, M. B. Maple, and K. A. Moler, Phys. Rev. B **81**, 214501 (2010).
[17] T. M. Rice and M. Sigrist, J. Phys.: Condens. Matter **7**, L643 (1995).
[18] J. F. Annett, G. Litak, B. L. Györffy, and K. I. Wysokiński, Phys. Rev. B **73**, 134501 (2006).
[19] C. M. Puetter and H.-Y. Kee, Europhys. Lett. **98**, 27010 (2012).
[20] S. Takamatsu and Y. Yanase, J. Phys. Soc. Jpn. **82**, 063706 (2013).
[21] K. Deguchi, Z. Q. Mao, H. Yaguchi, and Y. Maeno, Phys. Rev. Lett. **92**, 047002 (2004).
[22] T. Nomura and K. Yamada, J. Phys. Soc. Jpn. **69**, 3678 (2000).
[23] T. Nomura and K. Yamada, J. Phys. Soc. Jpn. **71**, 404 (2002).
[24] Y. Yanase and M. Ogata, J. Phys. Soc. Jpn. **72**, 673 (2003).
[25] T. Nomura, J. Phys. Soc. Jpn. **74**, 1818 (2005).
[26] Q. H. Wang, C. Platt, Y. Yang, C. Honerkamp, F. C. Zhang, W. Hanke, T. M. Rice, and R. Thomale, Europhys. Lett. **104**, 17013 (2013).
[27] S. Raghu, A. Kapitulnik, and S. A. Kivelson, Phys. Rev. Lett. **105**, 136401 (2010).
[28] S. B. Chung, S. Raghu, A. Kapitulnik, and S. A. Kivelson, Phys. Rev. B **86**, 064525 (2012).
[29] I. A. Firmo, S. Lederer, C. Lupien, A. P. Mackenzie, J. C. Davis, and S. A. Kivelson, Phys. Rev. B **88**, 134521 (2013).
[30] S. Raghu, S. A. Kivelson, and D. J. Scalapino, Phys. Rev. B **81**, 224505 (2010).
[31] S. Raghu and S. A. Kivelson, Phys. Rev. B **83**, 094518 (2011).
[32] S. Raghu, E. Berg, A. V. Chubukov, and S. A. Kivelson, Phys. Rev. B **85**, 024516 (2012).
[33] W. Cho, R. Thomale, S. Raghu, and S. A. Kivelson, Phys. Rev. B **88**, 064505 (2013).
[34] S. Raghu, S. B. Chung, and S. Lederer, J. Phys.: Conf. Ser. **449**, 012031 (2013).
[35] M. W. Haverkort, I. S. Elfimov, L. H. Tjeng, G. A. Sawatzky, and A. Damascelli, Phys. Rev. Lett. **101**, 026406 (2008).
[36] C. N. Veenstra, Z.-H. Zhu, M. Raichle, B. M. Ludbrook, A. Nicolaou, B. Slomski, G. Landolt, S. Kittaka, Y. Maeno, J. H. Dil, I. S. Elfimov, M. W. Haverkort, and A. Damascelli, Phys. Rev. Lett. **112**, 127002 (2014).
[37] H. Kontani, T. Tanaka, D. S. Hirashima, K. Yamada, and J. Inoue, Phys. Rev. Lett. **100**, 096601 (2008).
[38] K. K. Ng and M. Sigrist, Europhys. Lett. **49**, 473 (2000).
[39] See Supplemental Material at http://link.aps.org/supplemental/10.1103/PhysRevB.89.220510 for more details about the form of the spin-orbit coupling in the Ru atomic orbitals basis.
[40] Since both these parameters create repulsion between the bands, there is some freedom in their choice. Accordingly, our value of t''' is smaller than in calculations without SOC [23, 26] but is in agreement with a recent fit to ARPES data that includes SOC [59].
[41] A. P. Mackenzie, S. R. Julian, A. J. Diver, G. J. McMullan, M. P. Ray, G. G. Lonzarich, Y. Maeno, S. Nishizaki, and T. Fujita, Phys. Rev. Lett. **76**, 3786 (1996).
[42] E. Dagotto, T. Hotta, and A. Moreo, Phys. Rep. **344**, 1 (2001).
[43] W. Kohn and J. M. Luttinger, Phys. Rev. Lett. **15**, 524 (1965).
[44] S. Maiti and A. V. Chubukov, in *Lectures on the Physics of Strongly Correlated Systems, XVII: Seventeenth Training Course in the Physics of Strongly Correlated Systems*, edited by A. Avella and F. Mancini, AIP Conf. Proc. No. 1550 (AIP, Melville, NY, 2013), p. 3.
[45] See Supplemental Material in http://link.aps.org/supplemental/10.1103/PhysRevB.89.220510 for a survey of estimates for these parameters found in the literature [60, 61, 62, 63] .
[46] R. Balian and N. R. Werthamer, Phys. Rev. **131**, 1553 (1963).
[47] C. Kallin and A. J. Berlinsky, J. Phys.: Condens. Matter **21**, 164210 (2009).
[48] C. Kallin, Rep. Prog. Phys. **75**, 042501 (2012).
[49] H. Murakawa, K. Ishida, K. Kitagawa, Z. Q. Mao, and Y. Maeno, Phys. Rev. Lett. **93**, 167004 (2004).
[50] S. Kashiwaya, H. Kashiwaya, H. Kambara, T. Furuta, H. Yaguchi, Y. Tanaka, and Y. Maeno, Phys. Rev. Lett. **107**, 077003 (2011).
[51] H. Mukuda, K. Ishida, Y. Kitaoka, K. Miyake, Z. Q. Mao, Y. Mori, and Y. Maeno, Phys. Rev. B **65**, 132507 (2002).
[52] Y. Yoshioka and K. Miyake, J. Phys. Soc. Jpn. **78**, 074701 (2009).
[53] J. Jang, D. G. Ferguson, V. Vakaryuk, R. Budakian, S. B. Chung, P. M. Goldbart, and Y. Maeno, Science **331**, 186 (2011).
[54] K. Deguchi, Z. Q. Mao, and Y. Maeno, J. Phys. Soc. Jpn. **73**, 1313 (2004).
[55] S. Nishizaki, Y. Maeno, and Z. Mao, J. Phys. Soc. Jpn. **69**, 572 (2000).
[56] Y. Sidis, M. Braden, P. Bourges, B. Hennion, S. Nishizaki, Y. Maeno, and Y. Mori, Phys. Rev. Lett. **83**, 3320 (1999).
[57] I. Eremin, D. Manske, and K. H. Bennemann, Phys. Rev. B **65**, 220502 (2002).
[58] B. Béri, Phys. Rev. B **85**, 140501 (2012).
[59] V. Zabolotnyy, D. Evtushinsky, A. Kordyuk, T. Kim, E. Carleschi, B. Doyle, R. Fittipaldi, M. Cuoco, A. Vecchione, and S. Borisenko, J. Electron Spectrosc. Relat. Phenom. **191**, 48 (2013).
[60] L. Vaugier, H. Jiang, and S. Biermann, Phys. Rev. B **86**, 165105 (2012).
[61] J. Mravlje, M. Aichhorn, T. Miyake, K. Haule, G. Kotliar, and A. Georges, Phys. Rev. Lett. **106**, 096401 (2011).
[62] J.-W. Huo, T. M. Rice, and F.-C. Zhang, Phys. Rev. Lett. **110**, 167003 (2013).
[63] M. Behrmann, C. Piefke, and F. Lechermann, Phys. Rev. B **86**, 045130 (2012).